Fifth-order thermodynamic perturbation theory of uniform and nonuniform fluids

Shiqi Zhou
School of Physics Science and Technology, Central South University, Changsha, Hunan, China, 410083
(Received 26 September 2007; published 14 April 2008)

A recently proposed numerical third-order thermodynamic perturbation theory (TPT) is extended to its fifth-order counterpart. Extensive performance evaluation based on several model potentials indicates that the fifth-order version is generally superior to both the third-order version and a well-known second-order macroscopic compressibility approximation TPT, and is at least comparable to an accurate self-consistent Ornstein-Zernike integral equation approximation (SCOZA) with regard to predictions of varying bulk thermodynamic properties. A bulk second-order direct correlation function (DCF) free of numerical solution of a bulk OZ integral equation, is proposed, which, in combination with the framework of classical density functional theory (DFT) and a thermodynamic consistency condition, extends the uniform fifth-order TPT to nonuniform case. Grand canonical ensemble Monte Carlo simulation is carried out to produce density profile of a core-softened fluid confined in a hard spherical cavity, the resultant density profile is employed to evaluate the performance of the present nonuniform fifth-order TPT and a recently proposed third +second-order perturbation DFT. It is found that the present nonuniform fifth-order TPT is generally more accurate than the third+second-order perturbation DFT. Additional advantages of the present nonuniform fifth-order TPT over the third +second-order perturbation DFT is discussed.

DOI: 10.1103/PhysRevE.77.041110 PACS number(s): 61.20.Gy

I. INTRODUCTION

Since its inception [1], the thermodynamic perturbation theory (TPT) has been playing important role in calculation of bulk fluid thermodynamic properties, liquid-vapor transition [2], liquid-solid transition [3], and density functional theory (DFT) calculation [4]. Due to unavoidable truncation of the perturbation expansion, the TPT generally suffers from unaccuracy. Considering that the Ornstein-Zernike (OZ) integral equation theory (IET) is extremely inconvenient for calculation of liquid-vapor transition because of presence of the OZ IET nonsolution region, develpoing the TPT to a level of higher accuracy is a pressing task. Recently, a third-order TPT is proposed by the present author [5], it is found that the third-order TPT is more accurate than a conventional second-order TPT using a macroscopic compressibility approximation (MCA-TPT) [1(b)], first-order TPT [1(a)] and a self-consistent Ornstein-Zernike IET. However, for some potentials and thermodynamic quantities, the third-order TPT is still not very accurate, and significant deviation from simulational results still appears [6]. Therefore, a TPT with perturbation order higher than third-order is extremely welcome. In Ref. [5(a)], the uniform third-order TPT is extended to nonuniform square well (SW) fluid in the classical DFT framework, one of the inputs of the nonuniform third-order TPT is a tail part of a bulk second-order direct correlation function (DCF) for the potential under consideration. In Ref. [5(a)], the required tail part of the bulk second-order DCF is based on a mean spherical approximation (MSA), i.e., minus the tail part of the interaction potential scaled by $\beta=1/kT$ with k a Boltzmann constant and T the absolute temperature. In the present paper, we first extend the third-order TPT to its fifth-order version and the latter to its nonuniform counterpart, then we carry out grand canonical ensemble Monte Carlo simulation for a confined core-softened (CS) potential fluid, and obtain density profile of the confined core-softened potential fluid. Based on a comparison between the nonuniform fifth-order TPT and simulational data, we reexamine the validity of the MSA bulk second-order DCF and propose a new bulk second-order DCF. Validity of the nonuniform fifth-order TPT based on the new bulk second-order DCF is confirmed by comparing its density profile predictions with those of a previous third+second-order perturbation DFT and the simulational data available in literature and provided in the present paper.

The paper is organized as follows. In Sec. II, the uniform fifth-order TPT is explained in detail, then existing simulational data for several model potentials are employed to give a performance evaluation of the uniform fifth-order TPT. In Sec. III, we propose the nonuniform fifth-order TPT and the associated input, i.e., several bulk second-order DCFs expressions free from numerical solution of the OZ IET and their tail part. By comparing with the simulated density profiles of the confined CS potential fluid, we establish the correct choosing of the bulk second-order DCF and the tail part, and compare the resultant nonuniform fifth-order TPT with a recently proposed third+second-order perturbation DFT approach. Finally in Sec. IV, we discuss the advantages of the present nonuniform fifth-order TPT over the third+second-order perturbation DFT.

II. UNIFORM FIFTH-ORDER THERMODYNAMIC PERTURBATION THEORY

In the TPT, the excess Helmholtz free energy F_{ex} for a system of N particles in a volume V interacting via a full pair potential $u(r)$ is given by

$$F_{\text{ex}}(\rho_b) = F_{\text{ex-ref}}(\rho_b) + \sum_{n=1}^{\infty} \frac{1}{n!} N2\pi\rho_b \times \int drr^2 u_{\text{per}}(r) \left. \frac{\partial^{(n-1)} g(r,\xi,\rho_b,T)}{\partial \xi^{(n-1)}} \right|_{\xi=0}, \quad (1)$$

where, $\rho_b = N/V$ is the bulk number density, $F_{\text{ex-ref}}$ is the excess Helmholtz free energy of a reference hard sphere fluid with a potential u_{ref}, $u_{\text{per}}(r)$ is perturbation part of the whole potential $u(r)$ given by

$$u(r) = u_{\text{ref}}(r) + u_{\text{per}}(r). \quad (2)$$

In the present form of the TPT, $u_{\text{ref}}(r)$ is hard sphere potential given by

$$u_{\text{ref}}(r) = \infty, \quad r < \sigma,$$

$$0, \quad r > \sigma, \quad (3)$$

$g(r,\xi,\rho_b,T)$ is a radial distribution function (RDF) of the bulk fluid with pair potential $u(r;\xi)$ given by

$$u(r;\xi) = u_{\text{ref}}(r) + \xi u_{\text{per}}(r). \quad (4)$$

$\left. \frac{\partial^{(n-1)} g(r,\xi,\rho_b,T)}{\partial \xi^{(n-1)}} \right|_{\xi=0}$ is the $(n-1)$th derivative evaluated at $\xi=0$ of $g(r,\xi,\rho_b,T)$ with respect to ξ, $\left. \frac{\partial^0 g(r,\xi,\rho_b,T)}{\partial \xi^0} \right|_{\xi=0} = g(r,0,\rho_b)$ is the RDF of the hard sphere fluid of density ρ_b and diameter σ.

In the perturbation expansion, higher order terms are concerned with calculation of derivatives of the $g(r,\xi,\rho_b,T)$ with respect to ξ at $\xi=0$. In Ref. [5] One calculates these derivatives numerically by finite difference, this incurs calculation of $g(r,\xi,\rho_b,T)$ with $\xi=0, \pm\Delta\xi, \pm 2\Delta\xi$, here $\Delta\xi$ is a small increment, for example 0.01. Due to sensitivity of the finite difference derivatives on the numerical errors, calculation of $g(r,\xi,\rho_b,T)$ with $\xi=0, \pm\Delta\xi, \pm 2\Delta\xi$ only allows for reliable calculation of $\left. \frac{\partial^{(n-1)} g(r,\xi,\rho_b,T)}{\partial \xi^{(n-1)}} \right|_{\xi=0}$ for $n \leq 3$. To push the TPT to a higher order, for example, the present fifth-order, one has to calculate the $g(r,\xi,\rho_b,T)$ with $\xi = 0, \pm\Delta\xi, \pm 2\Delta\xi, \pm 3\xi, \pm 4\xi$. After acquirement of the $g(r,\xi,\rho_b,T)$ with $\xi=0, \pm\Delta\xi, \pm 2\Delta\xi, \pm 3\xi, \pm 4\xi$, the $\left. \frac{\partial^{(n-1)} g(r,\xi,\rho_b,T)}{\partial \xi^{(n-1)}} \right|_{\xi=0}$ for $n \leq 5$ can be obtained by numerical derivative. However, it should be pointed out that unlike in Ref. [5], where the $\left. \frac{\partial^{(n-1)} g(r,\xi,\rho_b,T)}{\partial \xi^{(n-1)}} \right|_{\xi=0}$ for $n \leq 3$ can be directly obtained by finite difference, for the present $\left. \frac{\partial^{(n-1)} g(r,\xi,\rho_b,T)}{\partial \xi^{(n-1)}} \right|_{\xi=0}$ with $n=4,5$, one has to beforehand smooth the $\left. \frac{\partial^2 g(r,\xi,\rho_b,T)}{\partial \xi^2} \right|_{\xi=0}$ data set which is mildly contaminated by the finite numerical derivative by a spline approximation, then employ the spline approximation for calculation of the $\left. \frac{\partial^{(n-1)} g(r,\xi,\rho_b,T)}{\partial \xi^{(n-1)}} \right|_{\xi=0}$ with $n=4,5$. As for the numerical solution of the OZ IET for $g(r,\xi,\rho_b,T)$, one can refer to Ref. [5].

The fifth-order TPT is given by

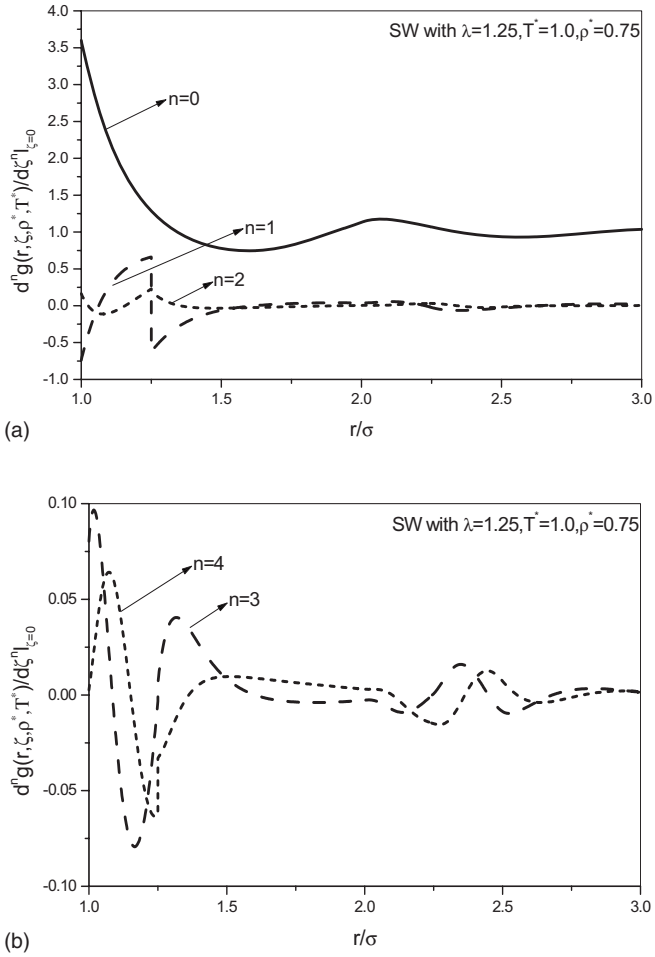

FIG. 1. The $\left. \frac{\partial^{(n)} g(r,\xi,\rho,T)}{\partial \xi^{(n)}} \right|_{\xi=0}$ for the SW fluid at one state point $(\lambda=1.25, T^*=1, \rho^*=0.75)$ for $n=0,1,2,3,4$.

$$F_{\text{ex}}(\rho_b) = F_{\text{ex-ref}}(\rho_b) + \sum_{n=1}^{5} \frac{1}{n!} N2\pi\rho_b \times \int drr^2 u_{\text{per}}(r) \left. \frac{\partial^{(n-1)} g(r,\xi,\rho_b,T)}{\partial \xi^{(n-1)}} \right|_{\xi=0}, \quad (5)$$

where $F_{\text{ex-ref}}(\rho_b)$ is given by a Carnahan-Starling equation of state [7].

To be more informative, we present the $\left. \frac{\partial^{(n-1)} g(r,\xi,\rho_b,T)}{\partial \xi^{(n-1)}} \right|_{\xi=0}$ for $n \leq 5$ in Figs. 1–3, the underlying potential is the hard sphere plus square well perturbation

$$u(r) = \infty, \quad r/\sigma \leq 1,$$

$$-\varepsilon, \quad \lambda \geq r/\sigma > 1,$$

$$0, \quad r/\sigma > \lambda. \quad (6)$$

Throughout the text, reduced temperature T^* is defined as kT/ε and reduced density ρ^* is defined as $\rho_b\sigma^3$. From Figs. 1 and 2 one sees that when the temperature T^* is not too low, the $\left. \frac{\partial^n g(r,\xi,\rho,T)}{\partial \xi^n} \right|_{\xi=0}$ with $n=3,4$ is small compared with their $n=0,1,2$ counterparts. Considering that as the order of the perturbation expansion increases, the coefficient $1/n!$ of the

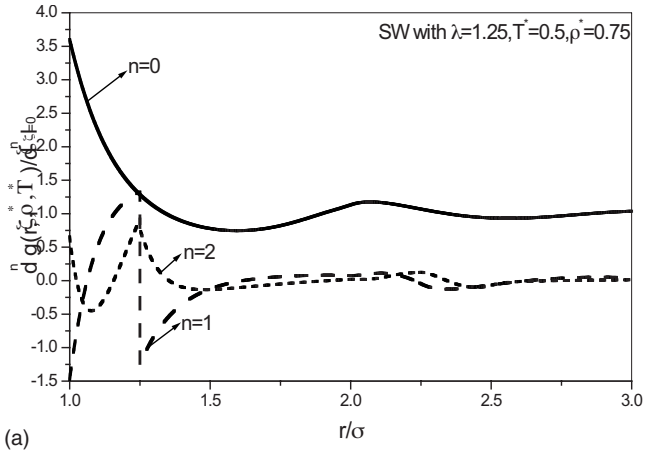

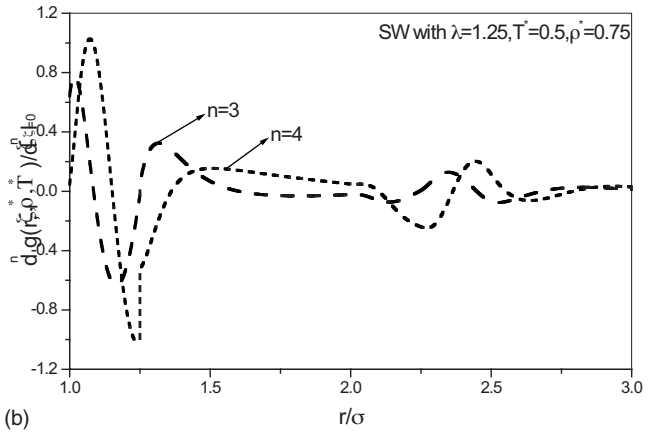

FIG. 2. The $\frac{\partial^{(n)}g(r,\xi,\rho,T)}{\partial\xi^{(n)}}|_{\xi=0}$ for the SW fluid at one state point ($\lambda=1.25, T^*=0.5, \rho^*=0.75$) for $n=0,1,2,3,4$.

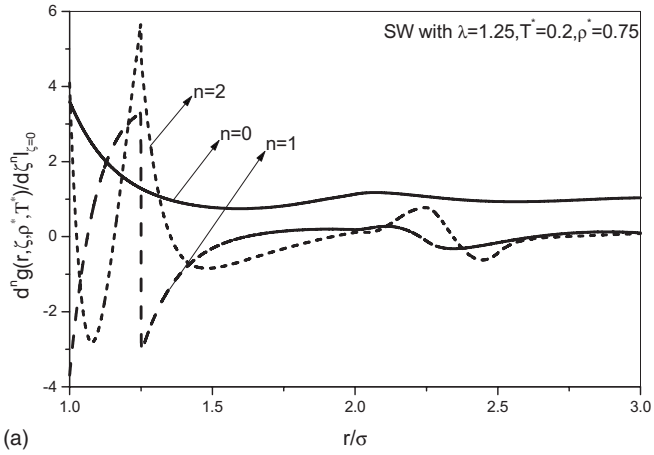

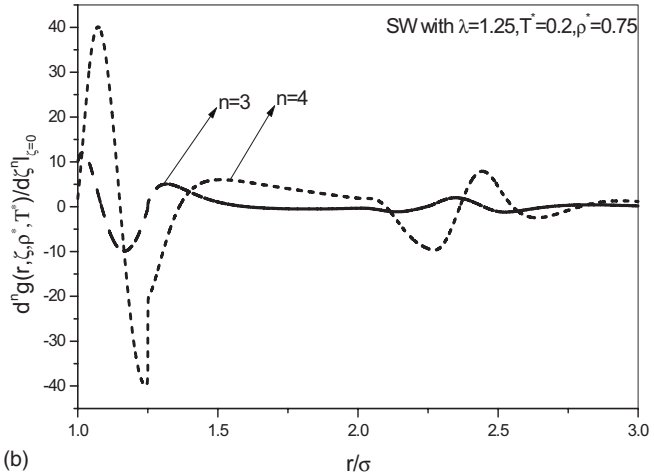

FIG. 3. The $\frac{\partial^{(n)}g(r,\xi,\rho,T)}{\partial\xi^{(n)}}|_{\xi=0}$ for the SW fluid at one state point ($\lambda=1.25, T^*=0.2, \rho^*=0.75$) for $n=0,1,2,3,4$.

corresponding expansion term also decreases, therefore the fourth- and fifth-order terms are negligibly small, the third-order TPT is sufficiently reliable for the higher temperature cases. As the temperature T^* decreases (see Fig. 2), the absolute value of $\frac{\partial^n g(r,\xi,\rho,T)}{\partial\xi^n}|_{\xi=0}$ with $n=3,4$ also increases to the extent that the absolute values of the fourth- and fifth-order terms become not negligible, addition of these two terms into the perturbation expansion will improve the accuracy of the TPT. When the T^* decreases furthermore (see Fig. 3), the $\frac{\partial^n g(r,\xi,\rho,T)}{\partial\xi^n}|_{\xi=0}$ with $n=3,4$ becomes unusually large, the absolute values of the fourth- and fifth-order terms will become far larger than those of their proceding terms, this indicates that the perturbation expansion may diverge for extremely low-temperature cases.

To confirm the accuracy of the uniform fifth-order TPT, we will investigate the thermodynamic properties of four model potentials given, respectively, as follows:

$$u(r) = \propto, \quad r/\sigma \le 1,$$

$$\varepsilon\delta, \quad b \ge r/\sigma > 1,$$

$$-\varepsilon, \quad c \ge r/\sigma > b,$$

$$0, \quad r/\sigma > c \tag{7}$$

for the CS potential with an internal repulsive core

$$u(r) = \propto, \quad r/\sigma \le 1,$$

$$= -\varepsilon(\sigma/r)^{\gamma}, \quad r\sigma > 1 \tag{8}$$

for the vdW potential

$$u(r) = \propto, \quad r\sigma \le 1,$$

$$-\varepsilon\delta, \quad b \ge r/\sigma > 1,$$

$$-\varepsilon, \quad c \ge r/\sigma > b,$$

$$0, \quad r/\sigma > c \tag{9}$$

for the CS potential with an internal attractive core

$$u(r) = \propto, \quad r/\sigma \le 1,$$

$$-\varepsilon\sigma \exp[-\kappa^*(r-\sigma)/\sigma]/r, \quad r/\sigma > 1 \tag{10}$$

for a hardcore attractive Yukawa (HCAY) potential.

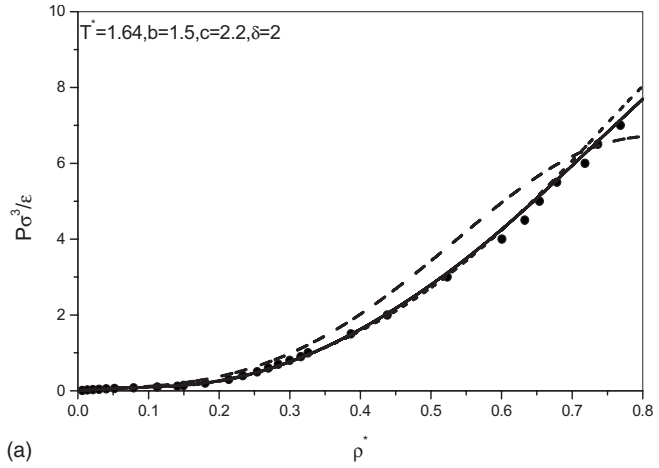

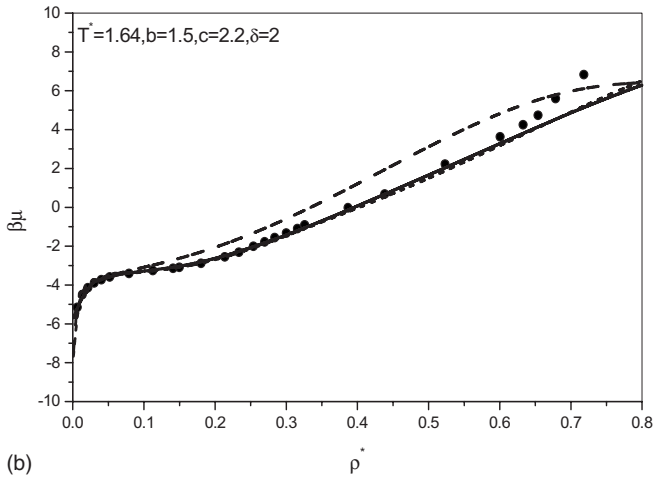

FIG. 4. The reduced pressure (a) and chemical potential (b) for the CS fluid with an internal repulsive core, the potential parameters are $T^*=1.64, b=1.5, c=2.2, \delta=2$. Symbols are for the simulational results [9], solid lines are for the uniform fifth-order TPT results, short dash lines are for the uniform third-order TPT results, while dash lines are for the second-order MCA-TPT results.

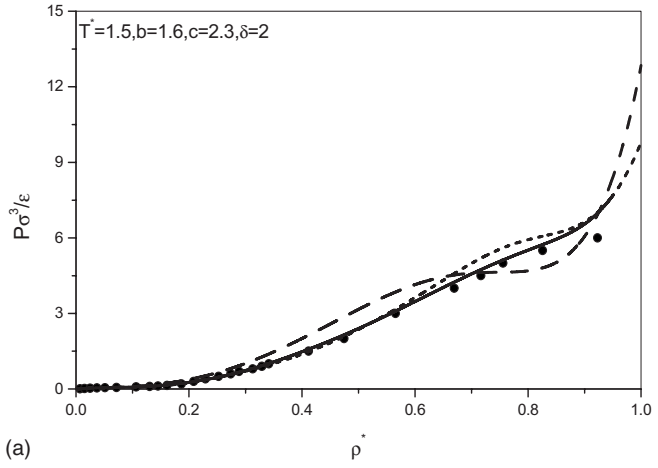

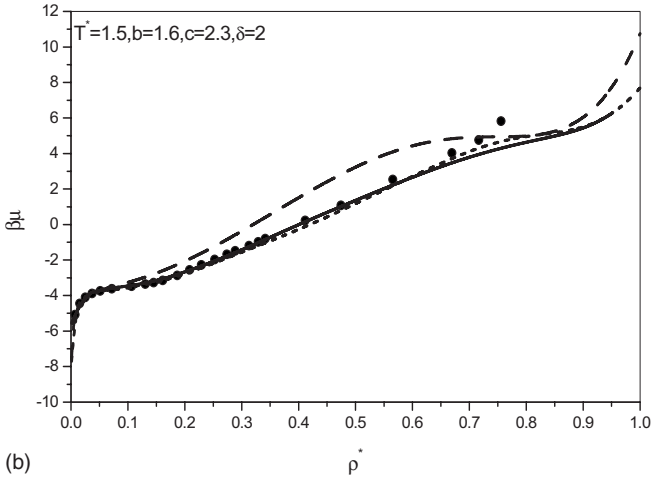

FIG. 5. The same as in Fig. 4 but $T^*=1.5$, $b=1.6$, $c=2.3$, $\delta=2$.

From the excess Helmholtz free energy $F_{ex}(\rho_b)$, one can obtain chemical potential μ and compressibility factor Z:

$$\beta\mu(\rho_b) = \frac{\partial}{\partial\rho_b}[\rho_b\beta f(\rho_b)], \tag{11}$$

$$Z(\rho_b) = \frac{\beta P}{\rho_b} = \beta\mu(\rho_b) - \beta f(\rho_b), \tag{12}$$

where $\beta f(\rho_b)=\beta F_{ex}(\rho_b)/N+(\ln\Lambda^3\rho_b-1)$ with Λ a thermal wavelength and P the pressure.

Figures 4–6 present the reduced pressure $P\sigma^3/\varepsilon=Z\rho^*T^*$ and reduced chemical potential $\beta\mu(\rho_b)$ as a function of the bulk density ρ^* for the CS potential with an internal repulsive core. One can see that the uniform fifth-order TPT is more accurate than the uniform third-order TPT, both the uniform fifth-order TPT and the uniform third-order TPT are superior to the well-known second-order MCA-TPT [1(b)] which is given by

$$F_{ex}(\rho_b) = F_{ex\text{-}ref}(\rho_b) + N2\pi\rho_b\int drr^2u_{per}(r)g(r,0,\rho_b) - N\beta^2\pi\rho_b\int drr^2u_{per}^2(r)g(r,0,\rho_b)\frac{1}{\beta}\left(\frac{\partial\rho_b}{\partial P}\right)_{ref}, \tag{13}$$

where $F_{ex\text{-}ref}(\rho_b)$ and the compressibility $\frac{1}{\beta}(\frac{\partial\rho_b}{\partial P})_{ref}$ of the reference hard sphere fluid are calculated by the Cananhan-Starling equation of state [7], a semianalytical expression for $g(r,0,\rho_b)$ [8] is employed only for use in Eq. (13).

It should be noted that although the uniform fifth-order TPT shows a clear improvement over the uniform third-order TPT in predicting the equation of state, in both cases there is a noticeable discrepancy between simulation and theoretical chemical potentials at high densities as recorded by Figs. 4–6. The reason is that with the "step" potentials, the rate of convergence was quite slow. This is because when two particles are moved within interaction range, the potential can change very rapidly (due to the steps), there is a low probability of accepting a move where two particles develop a strong, repulsive interaction. Therefore it is very difficult to

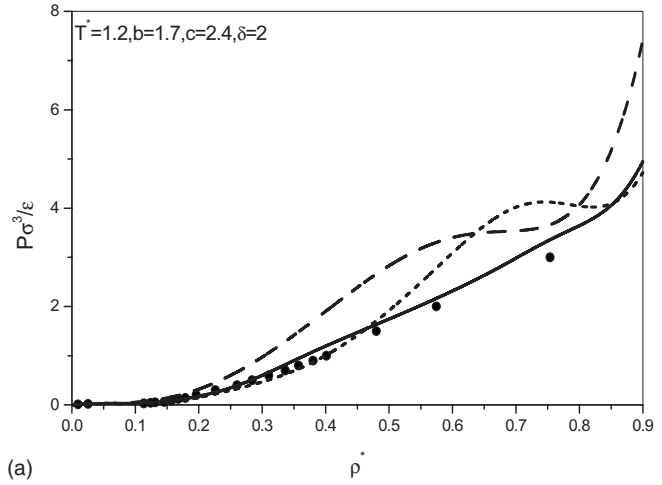

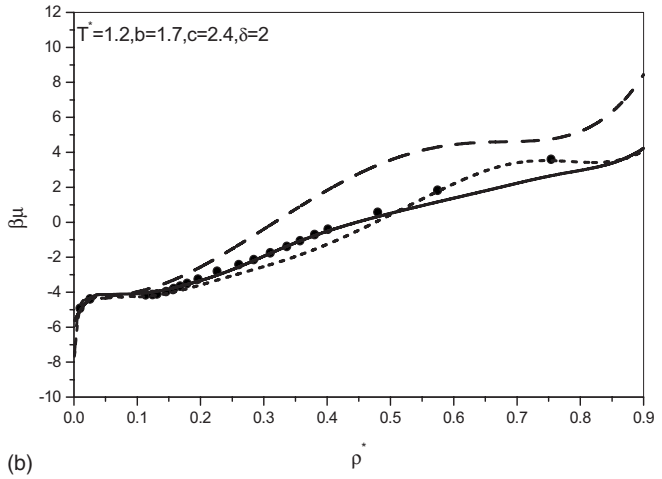

FIG. 6. The same as in Fig. 4 but $T^*=1.2$, $b=1.7$, $c=2.4$, $\delta=2$.

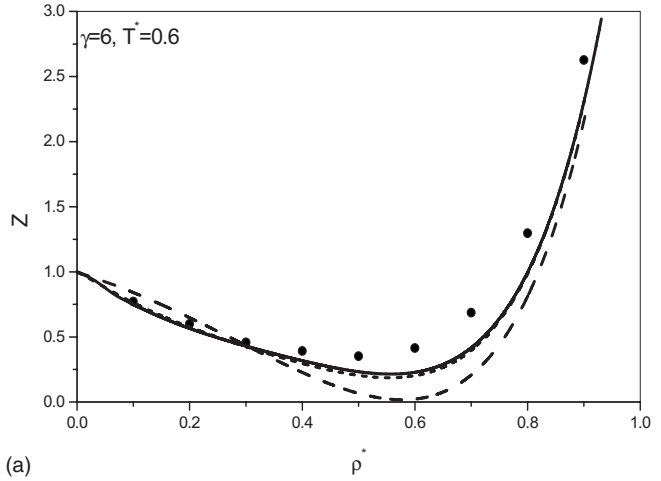

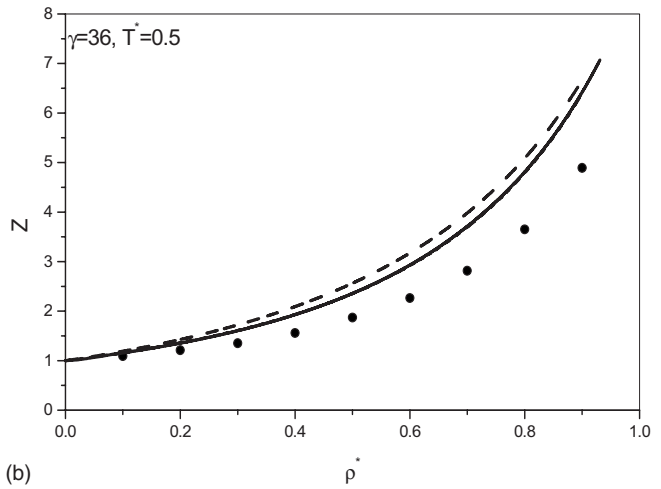

FIG. 7. The compressibility factor as a function of bulk density for the vdW fluid at $T^*=0.6$ and $\gamma=6$ (a), and $T^*=0.5$ and $\gamma=36$ (b). Symbols are for the simulational results [10], solid lines are for the uniform fifth-order TPT results, short dashed lines are for the uniform third-order TPT results, while dashed lines are for the second-order MCA-TPT results.

obtain the good statistics especially when the density is high. In fact, for the high density case there is an additional problem due to the possible existence of phase transitions which also leads to poor statistics.

Considering that the simulated temperatures in Figs. 4–6 are not low, but the uniform fifth-order TPT still performs obviously better than other two TPT versions, one can expext that the uniform fifth-order TPT will become significantly superior to the second-order MCA-TPT and the uniform third-order TPT for lower temperature cases.

In Fig. 7 the compressibility factors are presented for the vdW potential at two different combinations of potential parameter γ and reduced temperature T^*, one can see that for the continuous perturbation potential the uniform third-order TPT almost is of the same accuracy as the uniform fifth-order TPT, but both the uniform fifth-order TPT and the uniform third-order TPT are still superior to the second-order MCA-TPT even if for the simple and continuous perturbation tail the latter is very successful. It seems that the uniform third-order TPT is sufficiently accurate when the perturbation tail of the potential under consideration is continuous.

The liquid-vapor coexistence curves of the CS potential with an internal attractive core are presented in Fig. 8 for three different parameter combinations. Figure 8 clearly shows that the uniform fifth-order TPT is obviously superior to the uniform third-order TPT. The second-order MCA-TPT predictions severely deviate from the simulated coexistence curves [11].

The liquid-vapor coexistence curves of the HCAY potential are presented in Fig. 9 for two values of the screening parameter κ^*. Figure 9 shows that the simulational data from different literature for this potential deviates from each other, therefore it is very difficult to evaluate accurately the performance of both the uniform fifth-order TPT and the SCOZA [21]. Concretely speaking, for case of $\kappa^*=5$, the SCOZA is closer to the simulational data from Ref. [12] but deviates from the simulational data from Ref. [13]. On the contrary, the uniform fifth-order TPT is closer to simualtional data from Ref. [13] but deviates from the simulational data from Ref. [12]. For case of $\kappa^*=7$, it seems that on average the SCOZA predictions are closer to simulational data from various simulation [12,14,15] than the uniform fifth-order TPT

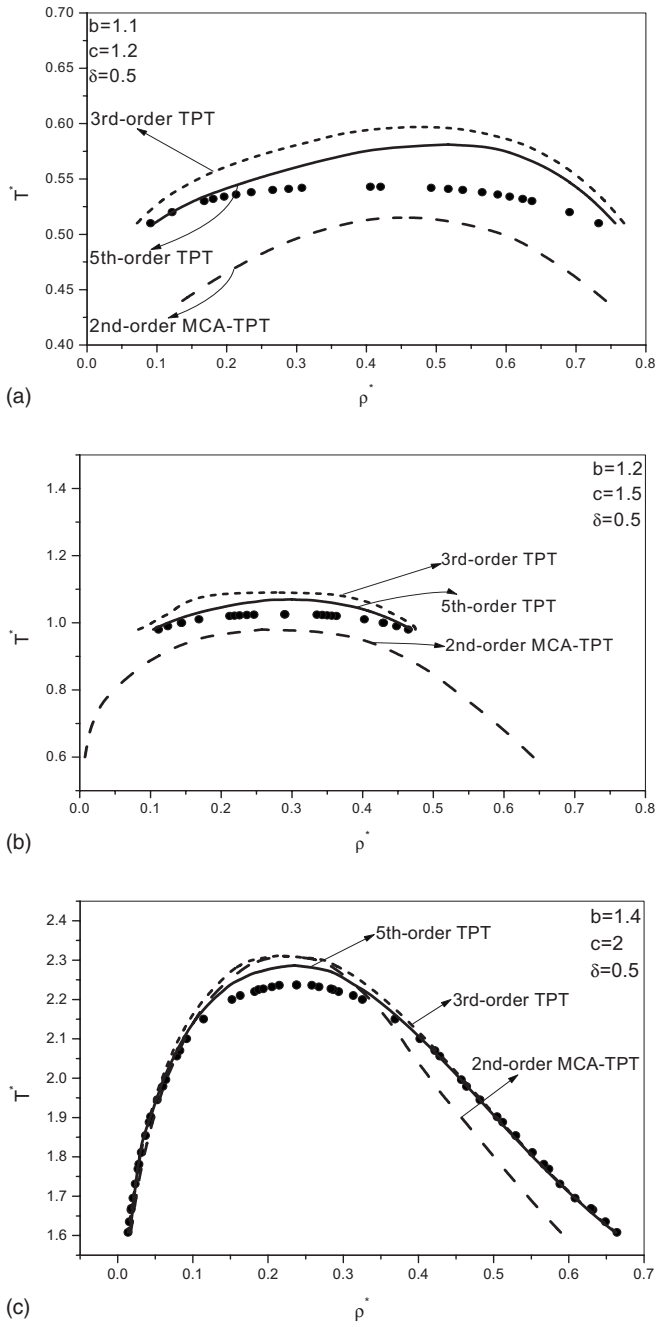

FIG. 8. The liquid-vapor coexistence curves for the CS fluid with an internal attractive core at several different parameter combinations $b=1.1$, $c=1.2$, $\delta=0.5$ for (a); $b=1.2$, $c=1.5$, $\delta=0.5$ for (b); and $b=1.4$, $c=2$, $\delta=0.5$ for (c). The symbols are for the simulational results [11]. Theoretical predictions from different routes are marked in the figures.

predictions. Although the two theoretical coexistence curves display some difference in the present scaling of the coordinate, the actual percent relative errors of the critical reduced temperature T^* are negligibly small, they are 2.75 for case of $\kappa^*=7$ and 2.12 for case of $\kappa^*=5$. For the SW fluid it is shown that the uniform third-order TPT [6] predicts the liquid-vapor coexistence curve more accurately than the SCOZA, one expects that the uniform fifth-order TPT will at least be more accurate than the SCOZA.

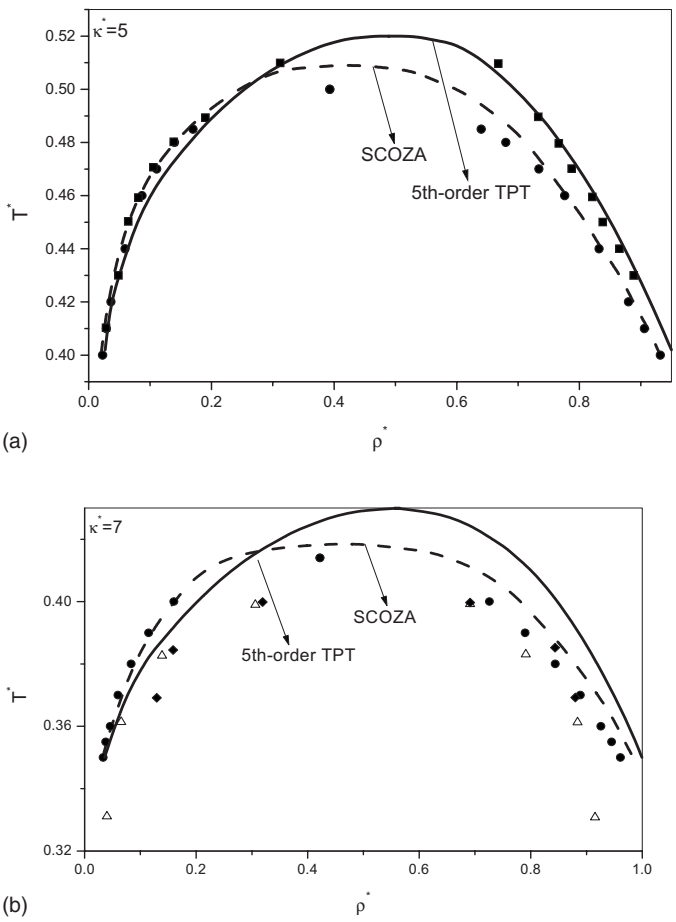

FIG. 9. The liquid-vapor coexistence curves for the HCAY fluid at two different screening parameter values $\kappa^*=5$ for (a) and $\kappa^*=7$ for (b). Theoretical predictions from two different routes are marked in the figures. The circles are for the simulational results obtained in Ref. [12], squares in Ref. [13], upangles in Ref. [14], and the diamonds in Ref. [15], the SCOZA curves are reproduced from Ref. [12].

III. NON-UNIFORM FIFTH-ORDER THERMODYNAMIC PERTURBATION THEORY

In Ref. [5(a)] the uniform third-order TPT is extended to nonuniform case in the framework of classical DFT in combination with a simple MSA bulk second-order DCF as weighting function for calculation of weighted density which is needed to construct the excess Helmholtz free energy density functional for the tail part of the potential under consideration. The nonuniform fifth-order TPT can be derived out following the same logic as in Ref. [5(a)], but the present investigation finds that the choice of the bulk second-order DCF plays keying role in the final accuracy of the nonuniform theory. Therefore we will propose new and more appropriate bulk second-order DCF.

In the classical DFT, the equlibrium density profile $\rho(\mathbf{r})$ is calculated by an Euler-Lagrange equation for the grand canonical potential

$$\rho(\mathbf{r}) = \rho_b \exp\{-\beta\varphi_{\text{ext}}(\mathbf{r}) + C^{(1)}(\mathbf{r};[\rho]) - C_0^{(1)}(\rho_b)\}, \quad (14)$$

where $C^{(1)}(\mathbf{r};[\rho])$ is first-order DCF of the nonuniform fluid, $C_0^{(1)}(\rho_b)$ is the uniform first-order DCF of the corresponding

coexistence bulk fluid of bulk density ρ_b, and $\varphi_{\text{ext}}(\mathbf{r})$ is an external potential responsible for formation of the density profile $\rho(\mathbf{r})$.

$C^{(1)}(\mathbf{r};[\rho])$ is mathematically first-order functional derivative of the excess Helmholtz free energy density functional $F_{\text{ex}}[\rho(\mathbf{r})]$ with respect to $\rho(\mathbf{r})$

$$C^{(1)}(\mathbf{r};[\rho]) = \frac{-\delta\beta F_{\text{ex}}[\rho]}{\delta\rho(\mathbf{r})} \tag{15}$$

in Ref. [5(a)] the $F_{\text{ex}}[\rho(\mathbf{r})]$ and corresponding $C^{(1)}(\mathbf{r};[\rho])$ are divided into hardcore part and tail part

$$F_{\text{ex}}[\rho(\mathbf{r})] = F_{\text{ex-hc}}[\rho(\mathbf{r})] + F_{\text{ex-tail}}[\rho(\mathbf{r})], \tag{16}$$

$$C^{(1)}(\mathbf{r};[\rho]) = C^{(1)}_{\text{hc}}(\mathbf{r};[\rho]) + C^{(1)}_{\text{tail}}(\mathbf{r};[\rho]), \tag{17}$$

correspondingly, one has

$$F_{\text{ex}}(\rho_b) = F_{\text{ex-hc}}(\rho_b) + F_{\text{ex-tail}}(\rho_b), \tag{18}$$

$$C^{(1)}_0(\rho_b) = C^{(1)}_{0\text{-hc}}(\rho_b) + C^{(1)}_{0\text{-tail}}(\rho_b), \tag{19}$$

and

$$C^{(1)}(\mathbf{r};[\rho]) - C^{(1)}_0(\rho_b) = [C^{(1)}_{\text{hc}}(\mathbf{r};[\rho]) - C^{(1)}_{0\text{-hc}}(\rho_b)] + [C^{(1)}_{\text{tail}} \times(\mathbf{r};[\rho]) - C^{(1)}_{0\text{-tail}}(\rho_b)]. \tag{20}$$

In Ref. [5(a)] the $F_{\text{ex-hc}}(\rho_b)=F_{\text{ex-ref}}(\rho_b)$ is assumed, and an adjustable parameter free version of the Lagrangian theorem-based density functional approximation (LTDFA) [16] is employed for the $F_{\text{ex-hc}}[\rho(r)]$. Therefore, one has

$$C^{(1)}_{\text{hc}}(\mathbf{r};[\rho]) - C^{(1)}_{0\text{-hc}}(\rho_b) = \int d\mathbf{r}_1[\rho(\mathbf{r}_1) - \rho_b]C^{(2)}_{0\text{-hs-PY}} \times\{|\mathbf{r}-\mathbf{r}_1|;\tilde{\rho}_{\text{hc}}[(\mathbf{r}+\mathbf{r}_1)/2,\lambda]\}, \tag{21}$$

where the hardcore weighted density

$$\tilde{\rho}_{\text{hc}}[(\mathbf{r}+\mathbf{r}_1)/2,\lambda] = \int d\mathbf{r}' C^{(2)}_{0\text{-hs-PY}}[|(\mathbf{r}+\mathbf{r}_1)/2-\mathbf{r}'|;\rho_b] \times\{\rho_b + \lambda[\rho(\mathbf{r}') - \rho_b]\}/C^{(1)}_{0\text{-hs-PY}}{}'(\rho_b). \tag{22}$$

In Eqs. (21), (22), $\lambda=1/2$. $C^{(n)}_{0\text{-hs-PY}}$ is the bulk hard sphere fluid nth-order DCF, $C^{(1)}_{0\text{-hs}}{}'(\rho_b)$ stands for first-order derivative of the bulk hard sphere fluid first-order DCF with respect to the density argument ρ_b. The subscript "PY" means that the $C^{(n)}_{0\text{-hs-PY}}$ and $C^{(1)}_{0\text{-hs-PY}}{}'(\rho_b)$ are obtained under Percus-Yevick approximation for the OZ integral equation.

As for the $C^{(1)}_{\text{tail}}(\mathbf{r};[\rho])$, Ref. [5(a)] proposes the following approximation for $F_{\text{ex-tail}}[\rho(r)]$,

$$F_{\text{ex-tail}}[\rho(\mathbf{r})] = \int d\mathbf{r}\rho(\mathbf{r}) f_{\text{ex-tail}}[\tilde{\rho}_{\text{tail}}(\mathbf{r})], \tag{23}$$

where $f_{\text{ex-tail}}$ is the bulk excess Helmholtz free energy per particle for the tail part. Considering that one has assumed $F_{\text{ex-hc}}(\rho_b)=F_{\text{ex-ref}}(\rho_b)$, we have

$$f_{\text{ex-tail}}(\rho_b) = F_{\text{ex-tail}}(\rho_b)/N = [F_{\text{ex}}(\rho_b) - F_{\text{ex-ref}}(\rho_b)]/N \tag{24}$$

weighted density $\tilde{\rho}_{\text{tail}}(\mathbf{r})$ is calculated by a simple weighted density approximation [17],

$$\tilde{\rho}_{\text{tail}}(\mathbf{r}) = \int d\mathbf{r}'\rho(\mathbf{r}')w(|\mathbf{r}-\mathbf{r}'|;\rho_b), \tag{25}$$

$$w(r;\rho_b) = C^{(2)}_{0\text{-tail}}(r;\rho_b) \Big/ \int d\mathbf{r} C^{(2)}_{0\text{-tail}}(r;\rho_b), \tag{26}$$

$C^{(2)}_{0\text{-tail}}(r;\rho_b)$ is the tail part of the bulk second-order DCF $C^{(2)}_0(r;\rho_b)$ of the full pair potential $u(r)$. In Ref. [5(a)] the tail part of a MSA is assumed for the $C^{(2)}_{0\text{-tail}}(r;\rho_b)$ for $r>\sigma$ and the $C^{(2)}_{0\text{-tail}}(r;\rho_b)$ is set to zero for $r<\sigma$, i.e.,

$$C^{(2)}_{0\text{-tail}}(r;\rho_b) = \begin{cases} 0, & r<\sigma, \\ -\beta u(r), & r\geq\sigma \end{cases} \tag{27}$$

in parallel with Eq. (15), one has

$$C^{(1)}_{\text{tail}}(\mathbf{r};[\rho]) = \frac{-\delta\beta F_{\text{ex-tail}}[\rho]}{\delta\rho(\mathbf{r})} = -\beta f_{\text{ex-tail}}[\tilde{\rho}_{\text{tail}}(\mathbf{r})] - \int d\mathbf{r}'\rho(\mathbf{r}')\beta f'_{\text{ex-tail}}[\tilde{\rho}_{\text{tail}}(\mathbf{r}')]w(|\mathbf{r}-\mathbf{r}'|;\rho_b) \tag{28}$$

imposing a limit of $\rho(\mathbf{r})\to\rho_b$ on $C^{(1)}_{\text{tail}}(\mathbf{r};[\rho])$, one obtains $C^{(1)}_{0\text{-tail}}(\rho_b)$,

$$C^{(1)}_{0\text{-tail}}(\rho_b) = \lim_{\rho(r)\to\rho_b} C^{(1)}_{\text{tail}}(\mathbf{r};[\rho]) = -\beta f_{\text{ex-tail}}(\rho_b) - \beta\rho_b f'_{\text{ex-tail}}(\rho_b). \tag{29}$$

Substituting Eqs. (20), (21), (28), (29), into Eq. (14), one obtains

$$\rho(\mathbf{r}) = \rho_b \exp\Big(-\beta\varphi_{\text{ext}}(\mathbf{r}) + \int d\mathbf{r}_1[\rho(\mathbf{r}_1)-\rho_b]C^{(2)}_0\{|\mathbf{r}-\mathbf{r}_1|;\tilde{\rho}_{\text{hc}}[(\mathbf{r}+\mathbf{r}_1)/2,\lambda]\} - \beta f_{\text{ex-tail}}[\tilde{\rho}_{\text{tail}}(\mathbf{r})] - \int d\mathbf{r}'\rho(\mathbf{r}')\beta f'_{\text{ex-tail}}[\tilde{\rho}_{\text{tail}}(\mathbf{r}')]w(|\mathbf{r}-\mathbf{r}'|;\rho_b) + \beta f_{\text{ex-tail}}(\rho_b) + \beta\rho_b f'_{\text{ex-tail}}(\rho_b)\Big). \tag{30}$$

In Eq. (30), $\tilde{\rho}_{\text{hc}}$ and $\tilde{\rho}_{\text{tail}}$ can be calculated respectively by Eqs. (22), (25).

When the uniform third-order TPT $F_{\text{ex}}(\rho_b)$ and fifth-order TPT $F_{\text{ex}}(\rho_b)$ are, respectively, substituted into Eq. (24), Eq. (30) is denoted, respectively, as nonuniform third-order TPT and nonuniform fifth-order TPT. If the Eq. (27) is used for the $C^{(2)}_{0\text{-tail}}(r;\rho_b)$, then the Eq. (30) is denoted respectively as nonuniform third-order TPT-MSA and nonuniform fifth-order TPT-MSA.

In Ref. [5(a)] the nonuniform third-order TPT-MSA is only tested by simulated density profiles of the SW fluid confined in a hard spherial cavity at two coexistence bulk states. To investiagte furthermore the validity and accuracy

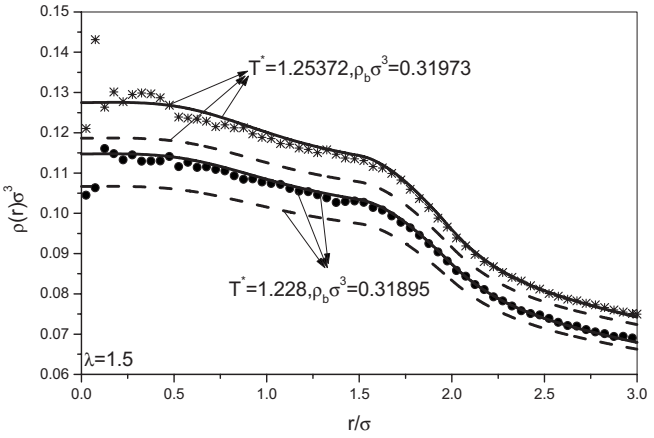

FIG. 10. Density profile of the SW fluid in the hard spherical cavity of radius $R=3.5\sigma$ in coexistence with the bulk fluid near the critical point. Symbols are for the GCEMC simulational results [5(a)], while solid lines are for the present nonuniform fifth-order TPT-MSA, dashed lines are for the nonuniform third-order TPT-MSA.

of the nonuniform TPT-MSA, and explore more accurate nonuniform TPT by proposing and using more appropriate $C^{(2)}_{0\text{-tail}}(r;\rho_b)$, we first carry out grand canonical ensemble Monte Carlo simulation (GCEMC) for the CS potential with an internal attractive core confined in a hard spherical cavity denoted by

$$\varphi_{\text{ext}}(r) = \infty, \quad r > R - 0.5\sigma,$$

$$=0, \quad r < R - 0.5\sigma. \tag{31}$$

It should be pointed out that by saying that the fluid confined in the spherical cavity is at coexistence with the bulk fluid, one means that the confined fluid is at the same temperature and chemical potential as the bulk fluid at the temperature and bulk density considered. The hard spherical cavity is chosen as sample external potential as it represents a stronger confinement on the fluid particles than a single hard wall or two hard walls separated by a small distance do and therefore constitutes a harsh test standard.

The GCEMC simulation is carried out at constant chemical potential μ, volume V, and temperature T. This set of independent parameters that defines the thermodynamic state of the system makes possible the study of equilibrium between the bulk fluid and that subjected to external fields originating from the presence of various spatial constrains. The general features of the GCEMC method are described elsewhere [18], some details peculiar to this study are discussed in several previous works [11,19].

The simulated coexistence bulk states are (1) $b=1.4$, $c=2$, $T^*=2.4$, $\delta=0.5$; (2) $b=1.2$, $c=1.5$, $T^*=1.55$, $\delta=0.5$; (3) $b=1.1$, $c=1.2$, $T^*=0.59$, $\delta=0.5$. For all of these cases, the coexistence bulk densities range from low values to high values. These simulational results, in combination with those published in Ref. [11], are sufficient to test the nonuniform TPT. We also will simulate the corresponding coexistence bulk pressures which are needed to determine an adjustable parameter in the recently proposed third+second-order perturbation DFT [11,19,20] which will be compared with the present nonuniform TPT. The simulated coexistence bulk pressures are collected in Table I.

TABLE I. Compressibility factor Z of the CS fluid with an internal attractive core at several states.

$b=1.4$, $c=2$, $T^*=2.4$, $\delta=0.5$					
$\rho_b\sigma^3$	0.10862800	0.32663700	0.50631600	0.73806300	0.81088100
Z	0.607230	0.342036	0.754325	2.37140	3.09172
$b=1.2$, $c=1.5$, $T^*=1.55$, $\delta=0.5$					
$\rho_b\sigma^3$	0.10336400	0.31745900	0.52380900	0.70221800	0.81008400
Z	0.867992	0.837736	1.46697	3.58699	5.88744
$b=1.1$, $c=1.2$, $T^*=0.59$, $\delta=0.5$					
$\rho_b\sigma^3$	0.11195700	0.31917200	0.51482400	0.71229500	0.81612500
Z	0.752016	0.492675	0.438860	0.805810	1.73260

We first compare the nonuniform third-order TPT-MSA and nonuniform fifth-order TPT-MSA with the corresponding simulational results in Fig. 10 for the confined SW fluid. It clearly shows that the fifth-order version accurately predicts the simulational results almost point by point, while the third-order version systematically deviates from the "exact" simulational results. This discloses the paramount importance of an accurate bulk $F_{\text{ex}}(\rho_b)$ as input into the present nonuniform version. In Fig. 10 there are noticeable discrepancies between the simulation and theoretical calculation as $r\to 0$. This significant disagreement can be ascribed to a low reliability of the simulation data for this regime stemming from a poor statistics of this part of the data. Namely, the density profile is determined from the average number of particles found within the spherical shells into which the spherical cavity is subdivided. As the volume of these shells decreases upon approaching the center of the cavity the counting statistics worsens in the same direction.

To confirm the global validity of the nonuniform TPT, we will employ the nonuniform fifth-order TPT-MSA for theo-

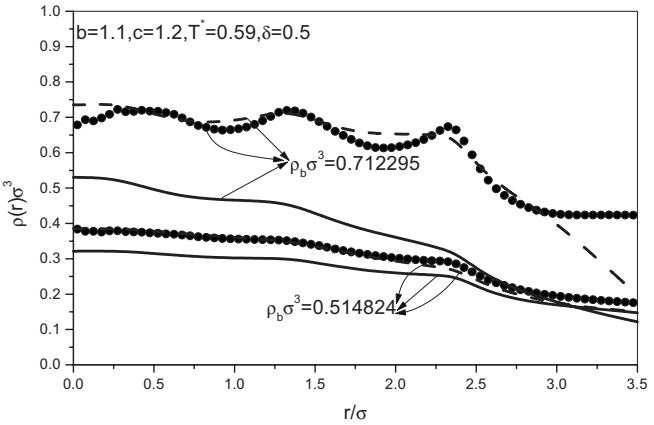

FIG. 11. Density profile of the CS fluid denoted by Eq. (9) in the hard spherical cavity of radius $R=4\sigma$ in coexistence with the bulk fluid ($b=1.1$, $c=1.2$, $T^*=0.59$, $\delta=0.5$), the bulk density is shown in the figure. Symbols are for the present GCEMC simulational results, while solid lines are for the present nonuniform fifth-order TPT-MSA, dashed lines are for the third+second-order perturbation DFT.

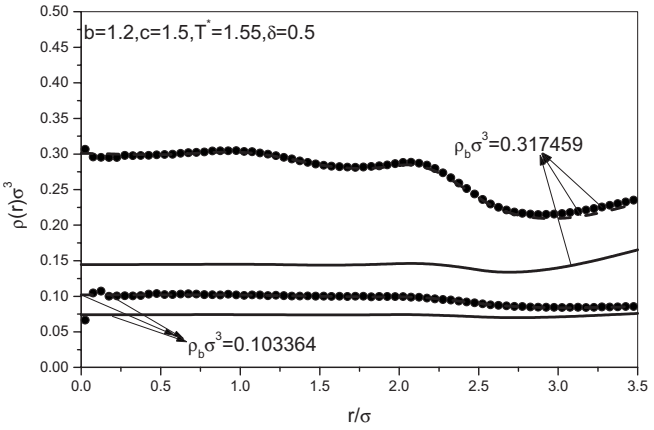

FIG. 12. The same as in Fig. 11 but with $b=1.2$, $c=1.5$, $T^*=1.55$, $\delta=0.5$ and different bulk densities.

retical calculation of the density profile of the CS fluid with an internal attractive core confined in the hard spherical cavity. We find that except for the three cases shown in Figs. 11, 12, 13 the nonuniform fifth-order TPT-MSA performs very satisfactorily. For the three cases in Figs. 11, 12, 13 the nonuniform fifth-order TPT-MSA systematically deviates from the simulational results while the third+second-order perturbation DFT performs satisfactorily.

It should be pointed out that in some of the figures, the dashed curves referred to in the caption cannot be made out. This is the case with the upper curves in Figs. 12, 13, and 15, the reason for this is that these curves are completely superimposed to either the points or the solid curves.

It would be interesting to explain the poor performance of the fifth order TPT-MSA theory with respect to the third +second-order perturbation DFT and simulation results in the cases of Figs. 11–13. As the accuracy of the uniform fifth-order TPT is confirmed, the origin of the poor performance for the particular cases comes from the low reliability of the Eq. (27) for the $C^{(2)}_{0\text{-tail}}(r;\rho_b)$. We propose three principles which guides for choosing approximation for the $C^{(2)}_{0\text{-tail}}(r;\rho_b)$. One is that the $C^{(2)}_{0\text{-tail}}(r;\rho_b)$ should conform with a zero density limit (ZDL) denoted by the following Eq. (32). The other is that the $C^{(2)}_{0\text{-tail}}(r;\rho_b)$ should not simply be set to zero, one should consider the "cross interaction" between the hardcore part and the tail part. The final one is that a negative value of the bulk second-order DCF is the characteristic of the repulsion interaction, the numerical value of the tail part $C^{(2)}_{0\text{-tail}}(r;\rho_b)$ should be positive. As will be illustrated, Only after all of the three principles are satisfied, does the resultant nonuniform TPT perform well for all cases.

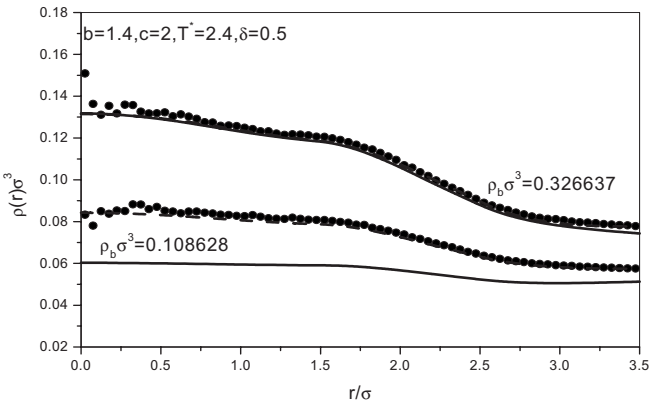

FIG. 13. The same as in Fig. 11 but with $b=1.4$, $c=2$, $T^*=2.4$, $\delta=0.5$, and different bulk densities.

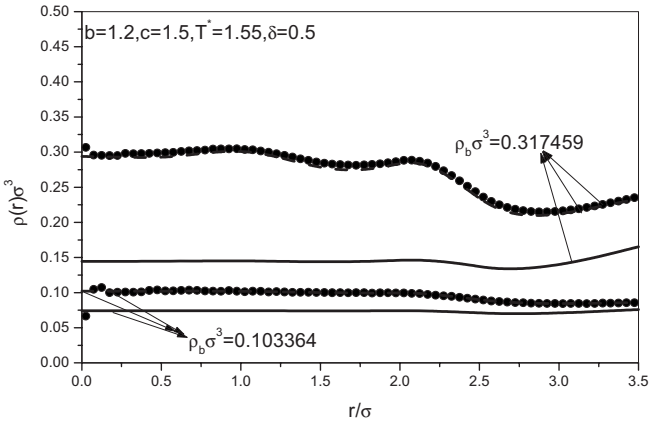

FIG. 14. Density profile of the CS fluid denoted by Eq. (9) in the hard spherical cavity of radius $R=4\sigma$ in coexistence with the bulk fluid ($b=1.2$, $c=1.5$, $T^*=1.55$, $\delta=0.5$), the bulk density is shown in the figure. Symbols are for the present GCEMC simulational results, while solid lines are for the present nonuniform fifth-order TPT-MSA, dashed lines are for the present nonuniform fifth-order TPT-ZDL.

Considering that the MSA $C^{(2)}_{0\text{-tail}}(r;\rho_b)$ denoted by Eq. (27) does not satisfy for a zero density limit denoted by Eq. (32)

$$C^{(2)}_{0\text{-tail}}(r;\rho_b)=0, \quad r<\sigma,$$
$$=\exp[-\beta u(r)]-1, \quad r\geq\sigma, \tag{32}$$

we now substitute Eq. (27) by Eq. (32) into the nonuniform version, the resultant approach is denoted by nonuniform fifth-order TPT-ZDL or nonuniform third-order TPT-ZDL. It is found that the nonuniform fifth-order TPT-ZDL performs same well for the SW fluid in Fig. 10 as the nonuniform fifth-order TPT-MSA does. Furthermore, as shown in Figs. 14 and 15, the nonuniform fifth-order TPT-ZDL improves the nonuniform fifth-order TPT-MSA for the cases shown in Figs. 12 and 13. However, as shown in Fig. 16, for the cases in Fig. 11 the nonuniform fifth-order TPT-ZDL almost predicts the same unsatisfactory results as the nonuniform fifth-order TPT-MSA does. In Fig. 17 we present one case where the nonuniform fifth-order TPT-ZDL performs very unsatisfactorily, while the nonuniform fifth-order TPT-MSA performs well for this case (not shown for brevity).

From physical view, although the Eq. (32) satisfies for the zero density limit condition, it is not thermodynamically self-consistent. To impose the thermodynamical self-consistency, we assume a following form for the $C^{(2)}_{0\text{-tail}}(r;\rho_b)$:

$$C^{(2)}_{0\text{-tail}}(r;\rho_b)=C^{(2)}_{0}(r;\rho_b)-C^{(2)}_{0\text{-hs-PY}}(r;\rho_b), \tag{33}$$

where $C^{(2)}_{0}(r;\rho_b)$ is assumed a following form:

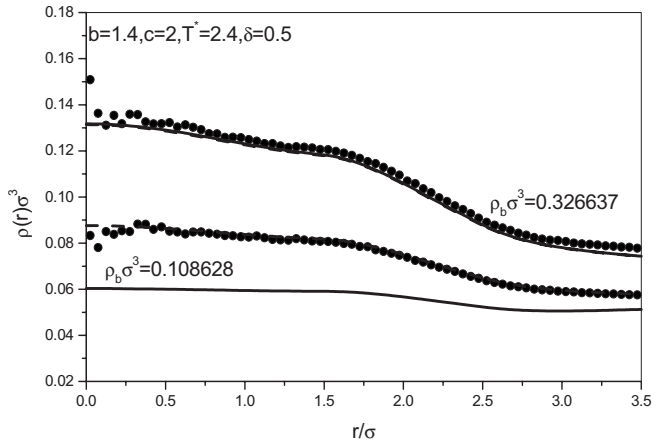

FIG. 15. The same as in Fig. 14 but with $b=1.4$, $c=2$, $T^*=2.4$, $\delta=0.5$ and different bulk densities.

$$C_0^{(2)}(r;\rho_b) = \chi C_{0\text{-hs-PY}}^{(2)}(r;\rho_b), \quad r < \sigma,$$

$$= \exp[-\beta u(r)] - 1, \quad r \geq \sigma \tag{34}$$

and the coefficient χ is determined by the thermodynamical self-consistency condition

$$1 - \rho_b \int d\mathbf{r} C_0^{(2)}(r;\rho_b) = 1/\chi_T = (\partial \beta P/\partial \rho_b)_T, \tag{35}$$

the pressure in the right-hand side of Eq. (35) is determined by differentiating with respect to the density the Helmholtz free energy given by Eq. (5) for the fifth-order TPT, or the corresponding expression for the third-order TPT. Therefore, Eq. (35) means a self-consistency between the excess Helmholtz free energy and the correlation function for each state point.

Considering that the $C_{0\text{-hs-PY}}^{(2)}(r;\rho_b)=0$ for $r>\sigma$, the Eqs. (33), (34) actually reduces to

$$C_{0\text{-tail}}^{(2)}(r;\rho_b) = \chi C_{0\text{-hs-PY}}^{(2)}(r;\rho_b) - C_{0\text{-hs-PY}}^{(2)}(r;\rho_b), \quad r < \sigma,$$

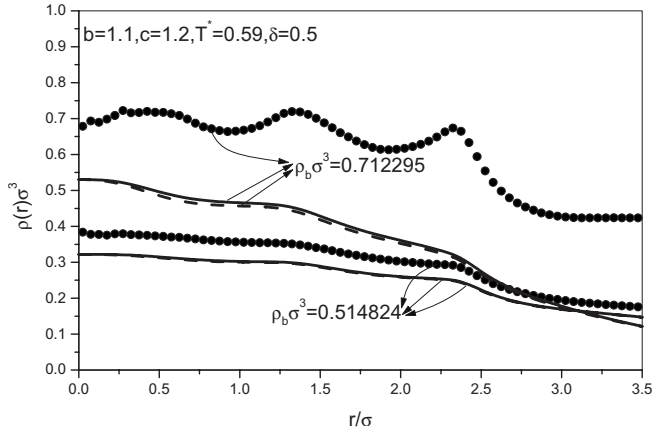

FIG. 16. The same as in Fig. 14 but with $b=1.1$, $c=1.2$, $T^*=0.59$, $\delta=0.5$ and different bulk densities.

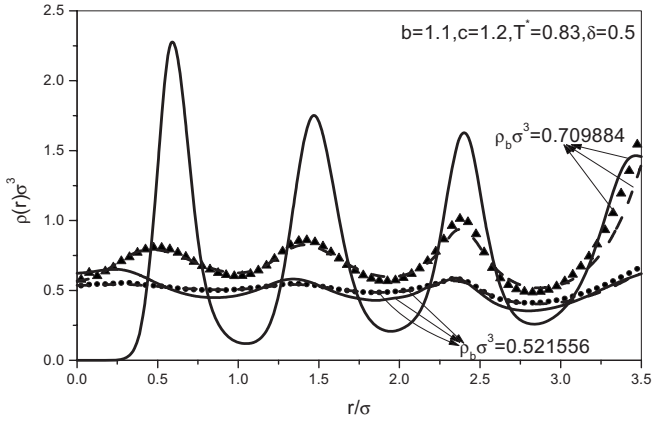

FIG. 17. Density profile of the CS fluid denoted by Eq. (9) in the hard spherical cavity of radius $R=4\sigma$ in coexistence with the bulk fluid ($b=1.1$, $c=1.2$, $T^*=0.83$, $\delta=0.5$), the bulk density is shown in the figure. Symbols are for the GCEMC simulational results [11], while solid lines are for the present nonuniform fifth-order TPT-ZDL, dashed lines are for the third+second-order perturbation DFT.

$$= \exp[-\beta u(r)] - 1, \quad r \geq \sigma. \tag{36}$$

When Eq. (36) is used in the nonuniform TPT versions, the resultant approaches are denoted, respectively, as nonuniform fifth-order TPT-ZDL-TS and nonuniform third-order TPT-ZDL-TS.

When the nonuniform fifth-order TPT-ZDL-TS is employed for the calculation of the confined SW fluid and CS fluid with an internal attractive core, for almost all of the cases where simulational results are available (including those unfavorable cases experienced by the nonuniform fifth-order TPT-ZDL and nonuniform fifth-order TPT-MSA), the nonuniform fifth-order TPT-ZDL-TS performs well, two unique exceptions occur in (1) the CS fluid with an internal attractive core $b=1.2$, $c=1.5$, $T^*=1.1$, $\delta=0.5$ with $\rho_b=0.710029$ and $\rho_b=0.80243$ and (2) the CS fluid with an internal attractive core $b=1.2$, $c=1.5$, $T^*=1.55$, $\delta=0.5$ with $\rho_b=0.70221800$ and $\rho_b=0.81008400$. For these exceptions it is very difficult to converge the final density profile, by careful iteration, the partial converged solution is even qualitatively incorrect. We find that for these unfavourable cases experienced by the nonuniform fifth-order TPT-ZDL-TS, the self-consistency parameter $\chi>1$, this means that $C_{0\text{-tail}}^{(2)}(r;\rho_b)<0$ for $r<\sigma$. In fact, the $C_{0\text{-tail}}^{(2)}(r;\rho_b)$ should usually be larger than zero for $r<\sigma$ as the $C_{0\text{-tail}}^{(2)}(r;\rho_b)$ for $r \geq \sigma$. Considering that the nonuniform fifth-order TPT-ZDL performs well when the $\chi>1$, for all of the unfavorable cases experienced by the nonuniform fifth-order TPT-ZDL, the $\chi<1$, and that for all cases where $\chi<1$ holds, the nonuniform fifth-order TPT-ZDL-TS performs well, we suggest a new self-consistency parameter χ_p to substitute the original χ in Eq. (36). The resultant new $C_{0\text{-tail}}^{(2)}(r;\rho_b)$ is given by

$$C_{0\text{-tail}}^{(2)}(r;\rho_b) = \chi_p C_{0\text{-hs-PY}}^{(2)}(r;\rho_b) - C_{0\text{-hs-PY}}^{(2)}(r;\rho_b), \quad r < \sigma,$$

$$= \exp[-\beta u(r)] - 1, \quad r \geq \sigma, \tag{37}$$

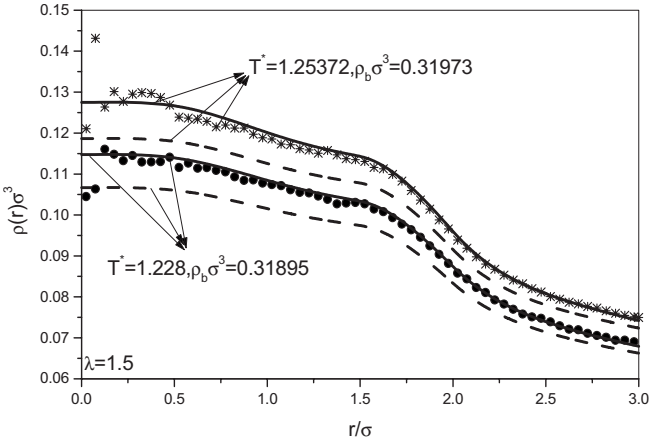

FIG. 18. Density profile of the SW fluid in the hard spherical cavity of radius $R=3.5\sigma$ in coexistence with the bulk fluid near the critical point. Symbols are for the GCEMC simulational results [5(a)], while solid lines are for the present nonuniform fifth-order TPT-ZDL-PTS, dashed lines are for the nonuniform third-order TPT-MSA.

$$\chi_p = \chi, \quad \chi \leq 1,$$

$$=1, \quad \chi > 1. \tag{38}$$

It should be pointed out that the self-consistency embodied in Eqs. (37), (38) is only partial, not global. With the Eqs. (37), (38) as input, the resultant nonuniform TPT is denoted as nonuniform fifth-order TPT-ZDL-PTS or nonuniform third-order TPT-ZDL-PTS.

The calculated results for the confined SW fluid and CS fluid with an internal attractive core by the nonuniform fifth-order TPT-ZDL-PTS are presented in Figs. 18–25 together with the corresponding simulational and other theory's results. We now will give a detailed performance comparison

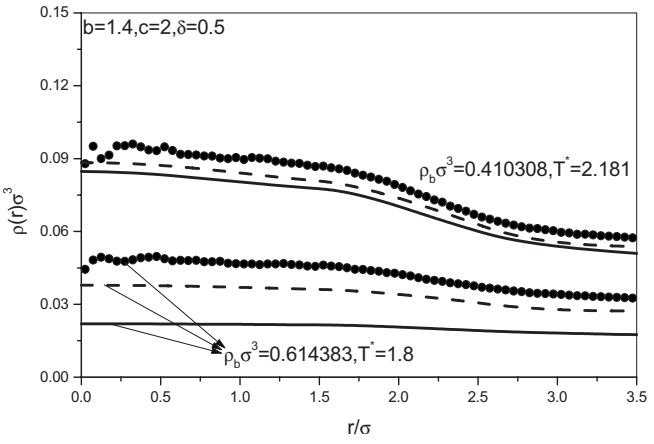

FIG. 19. Density profiles of the CS fluid ($b=1.4$, $c=2$, $\delta=0.5$) denoted by Eq. (9) in the hard spherical cavity of radius $R=4\sigma$ at supercritical reduced temperature and at different values of the bulk density as shown in the figure. The symbols are for the simulational results [11], solid lines are for the present nonuniform fifth-order TPT-ZDL-PTS, dashed lines are for the third+second-order perturbation DFT results [11].

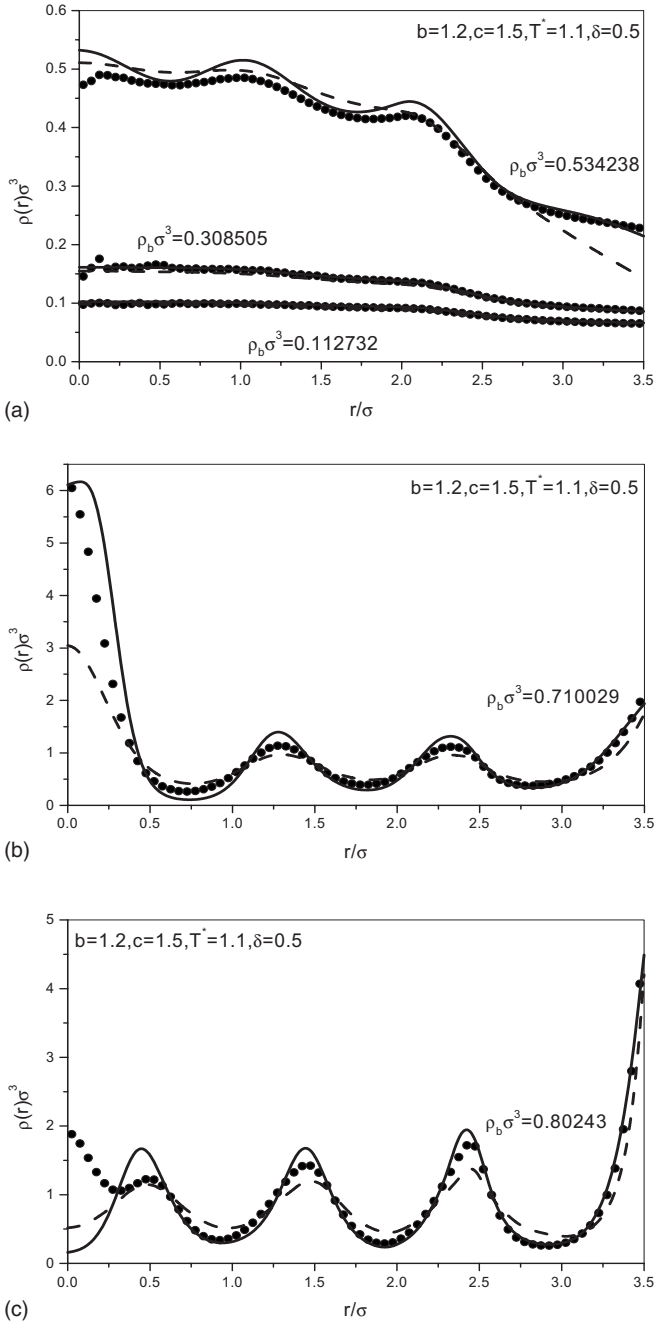

FIG. 20. The same as in Fig. 19 but with $b=1.2$, $c=1.5$, $T^*=1.1$, $\delta=0.5$ and different bulk densities.

between the present finally chosen nonuniform fifth-order TPT-ZDL-PTS and the previous third+second-order perturbation DFT.

Figure 18 shows that the nonuniform fifth-order TPT-ZDL-PTS accurately predicts the density profile of the confined SW fluid, while the nonuniform third-order TPT-MSA displays a whole displacement from the simulated density profile. Considering that the nonuniform fifth-order TPT-MSA and the nonuniform fifth-order TPT-ZDL also perform very well for this case, one concludes that high accuracy of the $F_{ex}(\rho_b)$ is a keying factor for the success of the resultant nonuniform TPT.

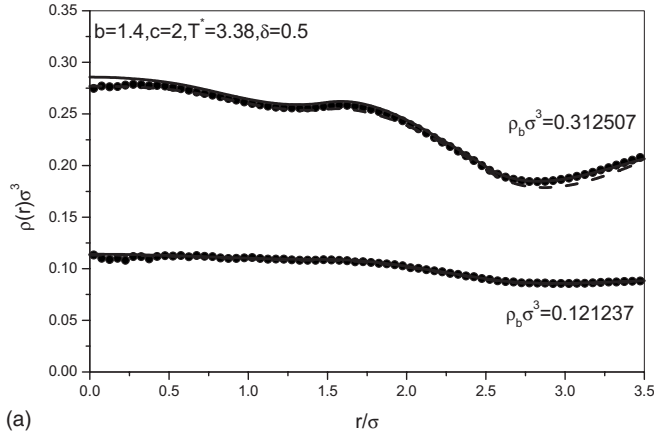

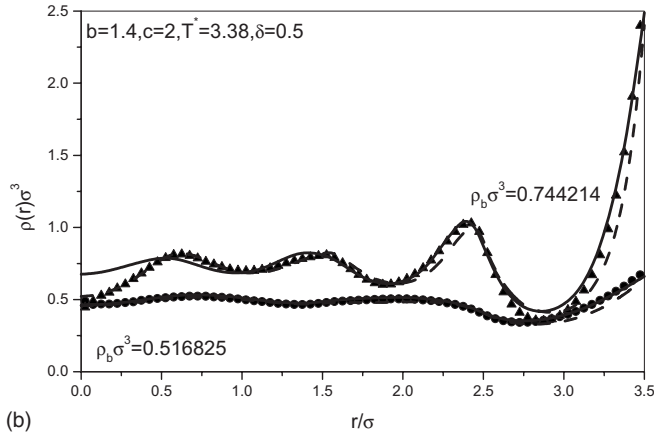

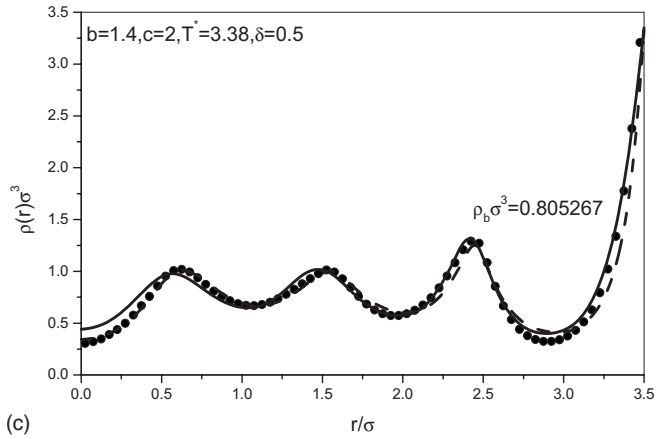

FIG. 21. The same as in Fig. 19 but with $b=1.4$, $c=2$, $T^*=3.38$, $\delta=0.5$ and different bulk densities.

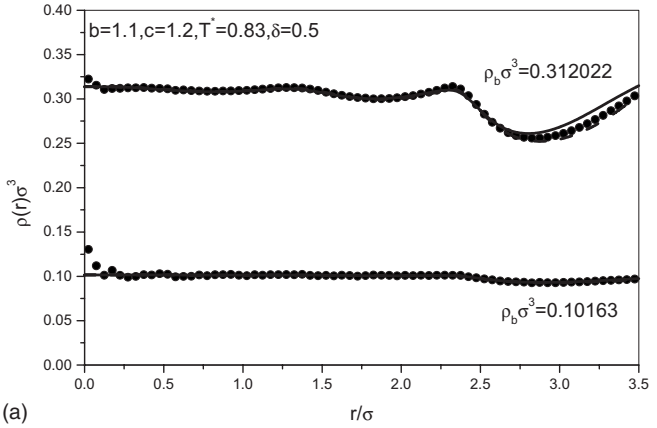

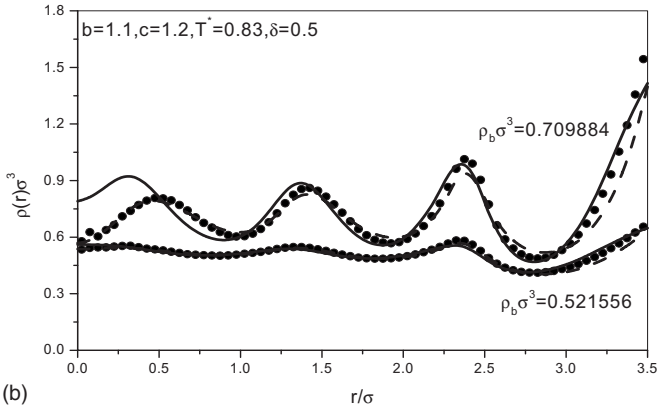

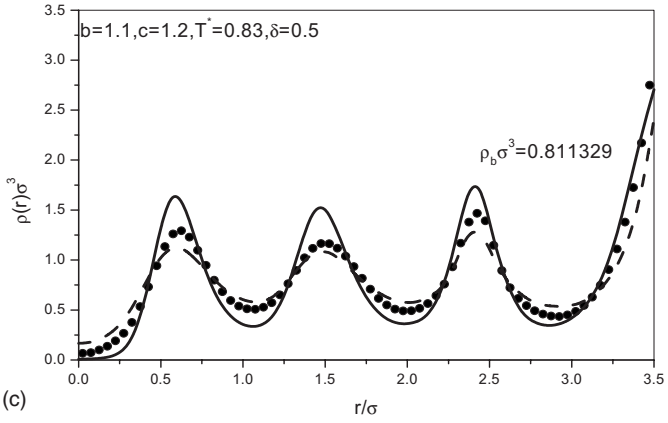

FIG. 22. The same as in Fig. 19 but with $b=1.1$, $c=1.2$, $T^*=0.83$, $\delta=0.5$, and different bulk densities.

Figure 19 shows that the nonuniform fifth-order TPT-ZDL-PTS predictions display a whole displacement from the corresponding simulational results, but the third+second-order perturbation DFT predictions are in closer agreement with the simulational results than the present predictions. Considering that the third+second-order perturbation DFT incorporates an adjustable parameter into itself, the adjustable parameter helps to adjust the whole position of the theoretical curve, the present nonuniform fifth-order TPT-ZDL-PTS is free of any adjustable parameter, and that the coexistence bulk state is near the gas-liquid coexistence curve or situated in the critical region of the bulk phase diagram, the small inaccuracy displayed for the present theory should be understood.

Figures 20, 21 show that for the intermediate range of $b=1.2$, $c=1.5$ and the long range of $b=1.4$, $c=2$ the nonuniform fifth-order TPT-ZDL-PTS achieves more accurate predictions than the third+second-order perturbation DFT does. While for a short range of $b=1.1$, $c=1.2$ the accuracy of the two approaches decreases a little as shown in Fig. 22, but the present nonuniform fifth-order TPT-ZDL-PTS is still (on average) superior to the third+second-order perturbation DFT.

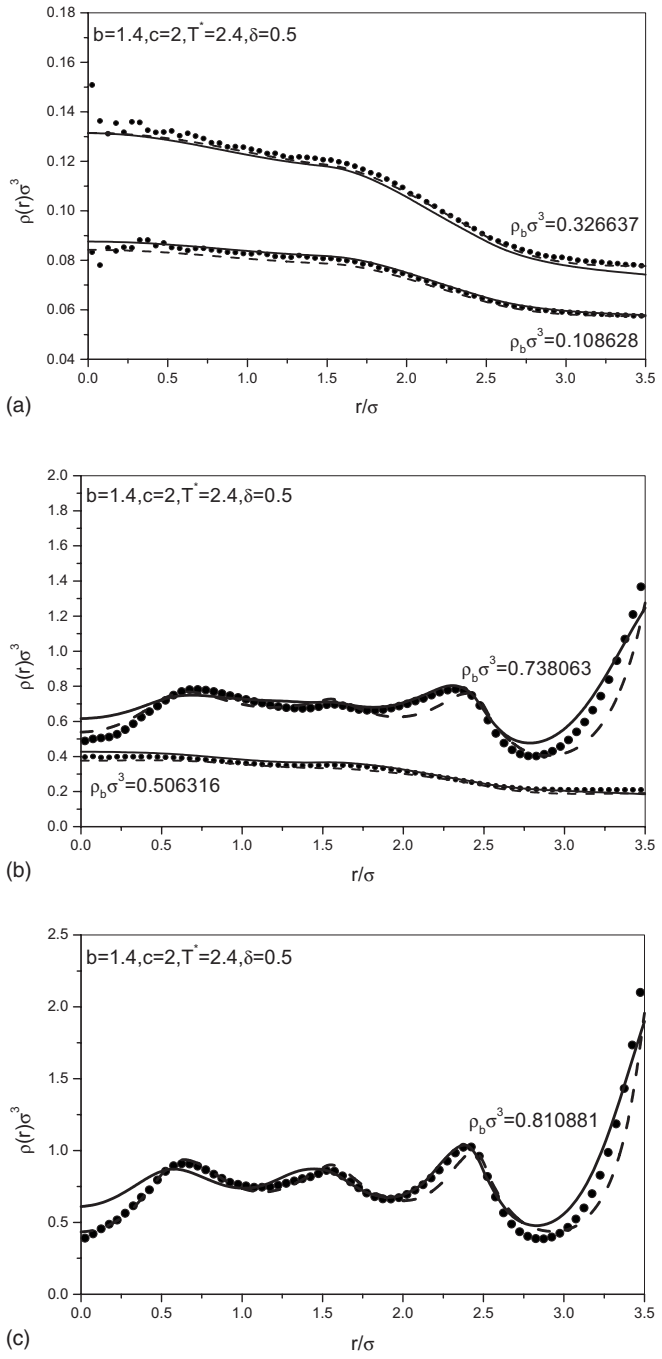

FIG. 23. Density profiles of the CS fluid ($b=1.4$, $c=2$, $T^*=2.4$, $\delta=0.5$) denoted by Eq. (9) in the hard spherical cavity of radius $R=4\sigma$ at supercritical reduced temperature and at different values of the bulk density as shown in the figure. The symbols are for the present simulational results, solid lines are for the present nonuniform fifth-order TPT-ZDL-PTS, dashed lines are obtained with help of the third+second-order perturbation DFT introduced in Ref. [11].

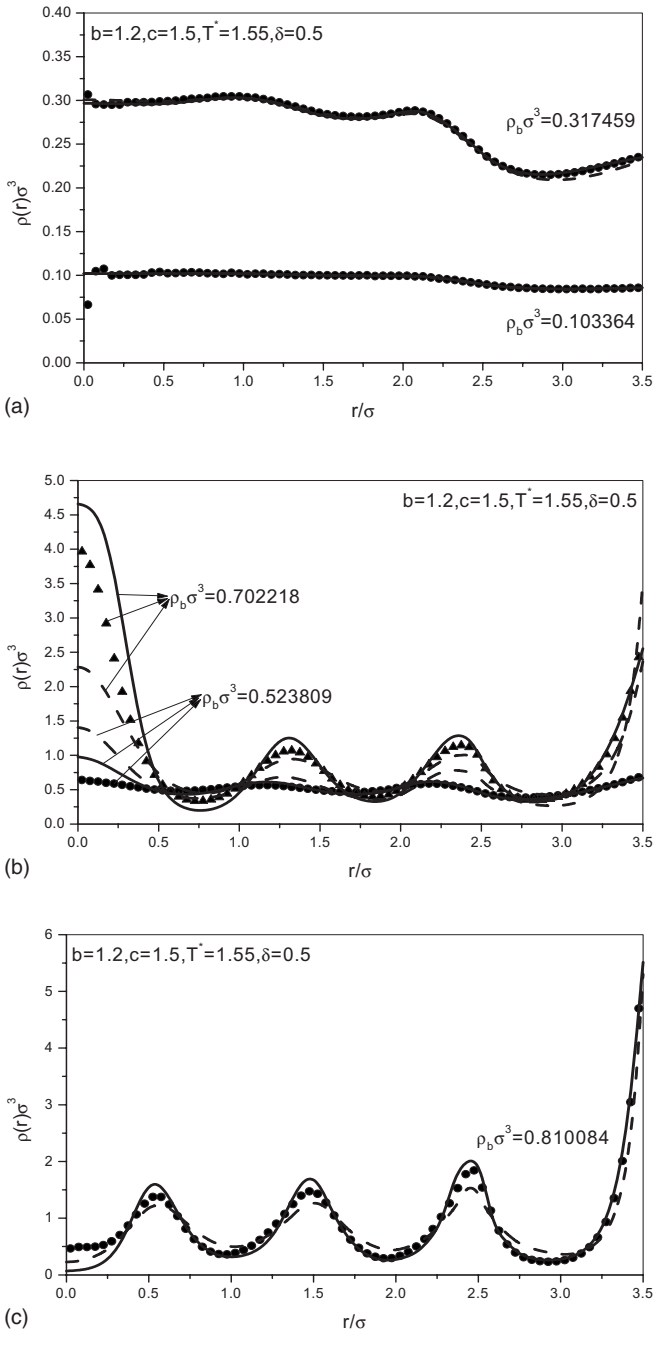

FIG. 24. The same as in Fig. 23 but with $b=1.2$, $c=1.5$, $T^*=1.55$, $\delta=0.5$ and different bulk densities.

Considering that the uniform TPT deteriorates as the potential range decreases, and the high accuracy of the $F_{ex}(\rho_b)$ is a keying factor for the success of the resultant nonuniform TPT as concluded above, the above phenomena can be understood easily.

Figures 23–25 display the comparison between the two theoretical approaches and the present simulational results. For the long-range potential (Fig. 23) the present nonuniform fifth-order TPT-ZDL-PTS generally is more accurate than the third+second-order perturbation DFT. For the intermediate range potential (Fig. 24), the present nonuniform fifth-order TPT-ZDL-PTS is obviously superior to the third+second-order perturbation DFT. For the short-range potential (Fig. 25), the accuracy of the present nonuniform fifth-order TPT-ZDL-PTS is a little inferior to the third+second-order perturbation DFT. This coincides with the above observation that the uniform TPT deteriorates as the potential range de-

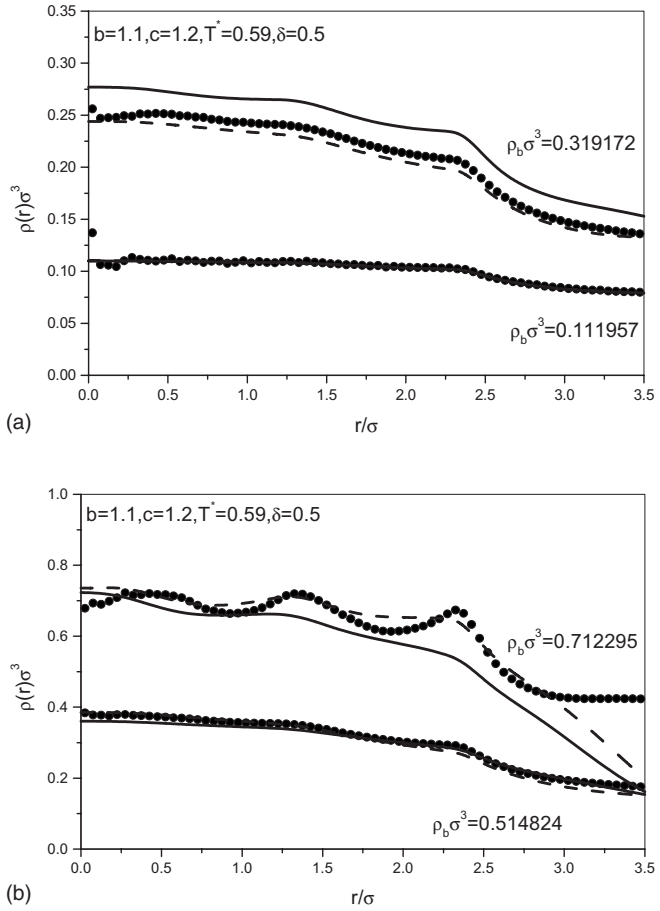

FIG. 25. The same as in Fig. 23 but with $b=1.1$, $c=1.2$, $T^*=0.59$, $\delta=0.5$ and different bulk densities.

creases, therefore the accuracy of the corresponding nonuniform TPT also deteriorates.

To conclude, one finds that the nonuniform fifth-order TPT-ZDL-PTS is a reliable approach, it is generally more accurate than the third+second-order perturbation DFT. For some cases, the nonuniform fifth-order TPT-ZDL-PTS is far more accurate than the third+second-order perturbation DFT, for the most unfavorable cases experienced by the former, the present approach is also at least comparable with the latter.

IV. SUMMARY

The recently proposed uniform third-order TPT [5,6] is extended to the fifth-order version for both uniform and nonuniform cases. It is indicated that the uniform fifth-order TPT is superior to the original third-order TPT and the existing second-order MCA-TPT. For case of the bulk HCAY fluid, the existing simulation data for the liquid-vapor coexistence curves deviate from each other, the uniform fifth-order TPT and the SCOZA are, respectively, in closer agreement with simulational results from one simulation than from other simulations. Totally speaking, the SCOZA is a little more accurate than the uniform fifth-order TPT for the HCAY fluid liquid-vapor coexistence curve, but the critical temperatures from the two routes are actually very near. Although the SCOZA is a little superior to the uniform fifth-order TPT for case of the HCAY liquid-vapor coexistence curve, the uniform third-order TPT is obviously superior to the SCOZA for case of the SW fluid liquid-vapor coexistence curves as shown in Ref. [6], let alone the present uniform fifth-order TPT.

As for the nonuniform fifth-order TPT version, we have illustrated that the success of the nonuniform version depends on the choosing of the tail part of the bulk second-order DCF. Only if the partial consistency is imposed on the bulk second-order DCF, can the nonuniform version be valid over all of the investigated cases. The partial consistency has taken four considerations into account. One is that the $C_0^{(2)}(r;\rho_b)$ should be in accord with the zero density limit. The other is that the $C_{0\text{-tail}}^{(2)}(r;\rho_b)$ for $r<\sigma$ should be larger or equal to zero. The third is that the $C_{0\text{-tail}}^{(2)}(r;\rho_b)$ cannot be simply equal to the $C_0^{(2)}(r;\rho_b)$ for $r\geq\sigma$ and zero for $r<\sigma$, it has to satisfy for the equality (33). Finally the thermodynamic self-consistency condition has to be imposed on the assumed $C_0^{(2)}(r;\rho_b)$, but when the imposition of the thermodynamic self-consistency condition leads to a negative $C_{0\text{-tail}}^{(2)}(r;\rho_b)$ for $r<\sigma$, the thermodynamic self-consistency condition should give place to the second consideration.

It should be acknowledged explicitly that the $C_0^{(2)}(r;\rho_b)$, whether it is from a combination of Eqs. (27) and $C_{0\text{-hs-PY}}^{(2)}(r;\rho_b)$, or from a combination of Eqs. (32) and the $C_{0\text{-hs-PY}}^{(2)}(r;\rho_b)$, or from Eq. (34), does not fulfill an exact requirement that the radial distribution function of the underlying potential fluid should vanish for $r<\sigma$. However, the undesriable violation of the exact requirement will not lead to very large error as the LTDFA [16,22] employed in the present paper has a self-correction efficacy [23] which can make good to some extent the shortcomings of the approximate bulk second-order DCF as input, and ensure the final theoretical results still satisfactory. Furthermore, unlike the case in Ref. [23] where the numerical value of the λ changes drastically when the bulk coexistence conditions change. For the present case the λ remains at 0.5 as required by the adjustable parameter free version [16] of the LTDFA [22], and the final theoretical results are still very satisfactory. The fortunate phenomenon has its physical origin which will be explained as follows. Unlike the case in Ref. [23] where reliability of the bulk second-order DCF for the polymer from solving numerically a polymer-RISM integral equation varies obviously as the bulk parameters change, therefore the dependence on self-correction efficacy of the LTDFA[22] also changes drastically, and this leads to a very dispersed numerical value of the λ, in the present case, the performance of the ansatz bulk second-order DCF is stable due to the imposition of the thermodynamic self-consistency condition, therefore the present λ value will not be dispersed. This explanation is furthermore evidenced by the observation made in Ref. [24], where it is shown that the λ still remains at 0.5 when the polymer-RISM integral equation bulk second-order DCF is scaled by a coefficient which is determined by the polymer equation of state combined with the isothermal compressibility equation. Scaling the bulk second-order DCF is also done in the present paper, the only difference is that the present unscaled bulk second-order

DCF is from several ansatzs for the DCF, but the unscaled bulk second-order DCF in Ref. [24] is from solving numerically polymer-RISM integral equation.

Another point which is worthwhile pointing out is that the weighted-density DFT used here for the tail part is not self-consistent, which means that the $C^{(2)}_{0\text{-tail}}(r;\rho_b)$ obtained by double functional differentiation of the given expression for the $F_{\text{ex-tail}}[\rho(\mathbf{r})]$ denoted by Eq. (23) will not coincide with that given by the ansatz adopted for $C^{(2)}_{0\text{-tail}}(r;\rho_b)$ as the weighting function in the functional $F_{\text{ex-tail}}[\rho(\mathbf{r})]$. The above mechanism concerning the radial distribution function self-consistency problem also explains the excusable existence of the small self-consistency problem of the weighted density approximation in a valid formalism as both the two self-consistency problems are concerned with correcting the likely unappropriateness of an approximate bulk second-order DCF by means of the self-correction efficacy [23] of the LTDFA [16,22] and by scaling the approximate bulk second-order DCF with a reliable equation of state.

One of the obvious advantages of the present nonuniform version over the previous theoretical approaches [11,19,20] is that the present nonuniform version is free of the numerical solution of the OZ IET, therefore it can be applied to the surface phase transition easily. The other is that not only the density profile can be calculated directly, but also the nonuniform free energy also can be calculated easily. After the density profile is obtained, one can directly obtain the $F_{\text{ex-tail}}[\rho(\mathbf{r})]$ from Eq. (23) and $F_{\text{ex-hc}}[\rho(\mathbf{r})]$ from the adjustable parameter free version of the LTDFA [16] based on a functional integration method [16], then the nonuniform free energy $F_{\text{ex}}[\rho(\mathbf{r})]$ can be obtained by Eq. (16). However, for the third+second-order perturbation DFT, the functional integration method cannot be applied to obtain the $F_{\text{ex}}[\rho(\mathbf{r})]$ when the temperature is below the critical temperature, the reason is simply that the functional integration method requires as input the bulk second-order DCF over the density range extending from the vapor phase side to liquid phase side of the liquid-vapor coexistence curve. However, the OZ integral equation has not physical solution inside the liquid-vapor coexistence region. As discussed above the difficulty of functional integration method disappears for the present nonuniform version for which the functional integration method is only applied for the hardcore part $F_{\text{ex-hc}}[\rho(\mathbf{r})]$ which is approximated by the hard sphere fluid whose bulk second-order DCF is available over the whole density range, for the tail part $F_{\text{ex-tail}}[\rho(\mathbf{r})]$ one can dispose of the functional integration method and directly use Eq. (22).

Further tests and applications of the present uniform and nonuniform fifth-order TPT are in progress which will be reported in separate publications.

ACKNOWLEDGMENTS

The author is pleased to acknowledge important comments from two reviewers. This project was supported by the National Natural Science Foundation of China (Grant No. 20673150).

[1] R. W. Zwanzig, J. Chem. Phys. **22**, 1420 (1954); J. A. Barker and D. Henderson, Rev. Mod. Phys. **48**, 587 (1976).
[2] L. W. Salvino and J. A. White, J. Chem. Phys. **96**, 4559 (1992); A. B. Adib, Phys. Rev. E **75**, 061204 (2007).
[3] Y. Choi, T. Ree, and F. H. Ree, J. Chem. Phys. **95**, 7548 (1991); S. Zhou, *ibid.* **127**, 084512 (2007).
[4] D. Henderson, *Fundamentals of Inhomogeneous Fluids* (Marcel Dekker, New York, 1992).
[5] S. Zhou, Phys. Rev. E **74**, 031119 (2006); J. Chem. Phys. **125**, 144518 (2006).
[6] S. Zhou, J. Phys. Chem. B **111**, 10736 (2007).
[7] N. F. Carnhan and K. E. Starling, J. Chem. Phys. **51**, 635 (1969).
[8] L. Verlet and J.-J. Weis, Phys. Rev. A **5** 939 (1972).
[9] P. J. Camp (unpublished).
[10] A. Diez, J. Largo, and J. R. Solana, J. Chem. Phys. **125**, 074509 (2006).
[11] S. Zhou, A. Jamnik, E. Wolfe, and S. V. Buldyrev, ChemPhysChem **8**, 138 (2007).
[12] Y. Duda, A. Romero-Martinez, and P. Orea, J. Chem. Phys. **126**, 224510 (2007).
[13] K. P. Shukla, J. Chem. Phys. **112**, 10358 (2000).
[14] M. Dijkstra, Phys. Rev. E **66**, 021402 (2002).
[15] M. H. J. Hagen and D. Frenkel, J. Chem. Phys. **101**, 4093 (1994).
[16] S. Zhou, Phys. Lett. A **319**, 279 (2003).
[17] S. Zhou, J. Chem. Phys. **110**, 2140 (1999).
[18] M. P. Allen and D. J. Tildesley, *Computer Simulation of Liquids* (Oxford University Press, New York, 1989).
[19] S. Zhou and A. Jamnik, Phys. Rev. E **73**, 011202 (2006).
[20] S. Zhou, Commun. Theor. Phys. **40**, 721 (2003).
[21] C. Caccamo, G. Pellicane, D. Costa, D. Pini, and G. Stell, Phys. Rev. E **60**, 5533 (1999).
[22] S. Zhou, New J. Phys. **4**, 36 (2002).
[23] S. Zhou, Chem. Phys. **310**, 129 (2005).
[24] S. Zhou, J. Colloid Interface Sci. **298**, 31 (2006).